A Wide-Speed High Torque Capability Utilizing Overmodulation Strategy in DTC of Induction Machines With Constant Switching Frequency Controller

Auzani Bin Jidin, *Member, IEEE*, Nik Rumzi Bin Nik Idris, *Senior Member, IEEE*, Abdul Halim Bin Mohamed Yatim, *Senior Member, IEEE*, Malik E. Elbuluk, *Senior Member, IEEE*, and Tole Sutikno, *Student Member, IEEE*

***Abstract*—This paper presents a simple overmodulation method employed in direct torque control (DTC) constant switching frequency (CSF) controller of induction machines. The proposed overmodulation method is utilized to extend a constant torque region and hence produce high torque capability in field-weakening region with six-step operation. It will be shown that the overmodulation operation using the DTC-CSF scheme can be established by controlling the stator flux locus from circular to the hexagonal shape. This is achieved by modifying the flux error status produced from the flux hysteresis controller before it is fed to the lookup table. The main benefit of the proposed method is its simplicity since it requires only a minor modification to the conventional DTC hysteresis-based structure and does not require a space-vector modulator.**

***Index Terms*—Direct torque control (DTC), field weakening, induction machine, overmodulation.**

I. Introduction

THE capability of induction machine drives to operate in overmodulation and field-weakening modes is very important in many industrial applications. It is desirable in order to achieve high constant power or the maximum torque capability over a wide speed range of operation.

Several papers have been published [1]–[14] proposing other types of solutions for achieving maximum torque capability in field-weakening region. The most common approach adopted is to estimate the optimal flux level of the motor based on the maximum values of inverter voltage and inverter current. Typically, the algorithms used require frame transformer, knowledge of machine parameters, and space-vector modulator. For example, Sang-Hoon and Seung-Ki [3] used field-oriented control space-vector modulation (FOC-SVM) that considers voltage and current limit conditions to compute the controllable currents (in stator flux reference frame) in achieving the appropriate flux level in field-weakening region. Other papers have reported a robust field-weakening strategy, so that any variations of machine parameters used in calculating the optimal flux, can be compensated [5], [9], [11], [14].

In general, the SVM technique is employed to exploit the inverter voltage into the overmodulation region where the voltage reference is normally used to define the mode of overmodulation [15]. The ability of SVM to fully utilize the available inverter voltage mainly depends on the vector control strategy to produce the maximum possible voltage reference while simultaneously maintaining the regulation of flux and torque. Various methods have been proposed to estimate the voltage reference [13], [16]–[22]; for instance, in the case of direct torque control (DTC)-SVM, Tripathi *et al*. [17] utilized predictive control of stator flux error vector to estimate the reference voltage. Habetler *et al*. [16] used dead-beat control, with several complicated equations, to generate the reference voltage in real time. Among the various schemes only [12] and [13] can achieve maximum torque capability in field-weakening region with six-step voltage operation. In [12], due to the hexagonal shape of the stator flux locus, the current contains low-frequency harmonic components even when the drive is operating in steady-state condition. On the other hand, Tripathi *et al*. [13] achieved the six-step mode operation through overmodulation using SVM. Ultimately, all of the proposed methods [13], [16]–[18], [21], [22] complicate the basic control structure of DTC drive systems as originally proposed in [23].

Until now, no study has been reported to carry out the overmodulation strategy in DTC hysteresis-based structure mainly due to the fact that in DTC hysteresis-based structure, unlike the DTC-SVM, there is no voltage reference available. This paper presents a simple overmodulation strategy employed in DTC constant switching frequency (CSF)-based induction machines. The control structure of DTC-CSF is similar to the DTC hysteresis-based scheme [36], which does not use SVM and, hence, does not have the voltage vector reference to operate in overmodulation modes [15]. However, unlike the DTC-hysteresis-based scheme, DTC-CSF can be operated with CSF. It will be shown in this paper that even without SVM, the

Manuscript received June 24, 2010; revised November 8, 2010, February 27, 2011, and September 5, 2011; accepted September 6, 2011. Date of current version February 27, 2012. Recommended for publication by Associate Editor F. Blaabjerg.

A. B. Jidin, N. R. B. N. Idris, A. H. B. M. Yatim, and T. Sutikno are with the Department of Energy Conversion, Universiti Teknologi Malaysia, Skudai, 81310 Johor, Malaysia (e-mail: ajudin@fke.utm.my; nikrumzi@fke.utm.my; halim@ieee.org; tsutinko@fke.utm.my).

M. Elbuluk is with the Department of Electrical and Computer Engineering, University of Akron, Akron 44325-3904 OH USA (e-mail: melbuluk@uakron.edu).

Color versions of one or more of the figures in this paper are available online at http://ieeexplore.ieee.org.

Digital Object Identifier 10.1109/TPEL.2011.2168240

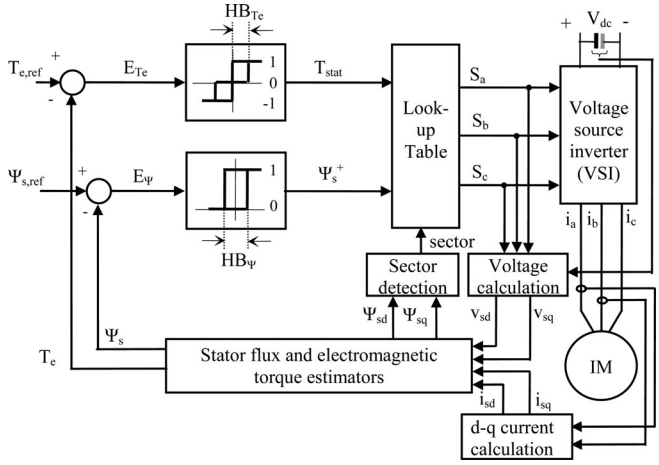

Fig. 1. Structure of basic DTC-hysteresis-based induction machine.

inverter voltage can be gradually transformed from pulsewidth modulation (PWM) to six-step mode by changing the stator flux locus from circular to hexagonal shapes. In this way, an extension of constant torque region can be achieved which results in higher torque capability in field-weakening region. By using this technique, it is also possible for the drive to operate in six-step mode during acceleration (and deceleration) and revert back to the PWM mode when steady-state condition is reached, for beyond based speed operation. In Section II, the DTC with constant frequency torque controller is briefly discussed. Section III explains the torque capability in DTC and describes how the overmodulation is achieved based on stator flux locus transformation. Section IV presents improved torque capability with the proposed overmodulation strategy. Section V describes the proposed control structure. Section VI presents the hardware implementation and experimental results of the proposed method. Finally, the conclusion is given in Section VII.

II. DTC With CSF Scheme

Unlike FOC, the DTC scheme as shown in Fig. 1, offers a simple control structure wherein the torque and flux can be separately controlled using three-level and two-level hysteresis comparators, respectively. The output of the comparators and the stator flux angle are used to index a lookup table of optimum voltage vector as proposed in [23], to determine the appropriate voltage vectors to control both torque and flux. However, the hysteresis torque controller utilized in the basic DTC structure results in two major disadvantages, namely variable inverter switching frequency and high torque ripple. Several methods have been proposed to overcome these problems. For example, the problems were minimized by the use of variable hysteresis band [24], [25], dithering technique [26], controlled duty ratio cycle technique [27], [28], space-vector modulation (DTC-SVM) [21], [29]–[31], and most recently the use of predictive control [32]–[35].

An attempt was made to reduce the torque ripple by replacing the torque hysteresis controller with constant frequency torque controller as depicted in Fig. 2 [36]. In such a way, the

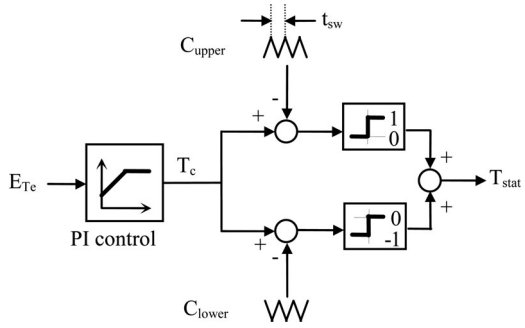

Fig. 2. Constant frequency torque controller.

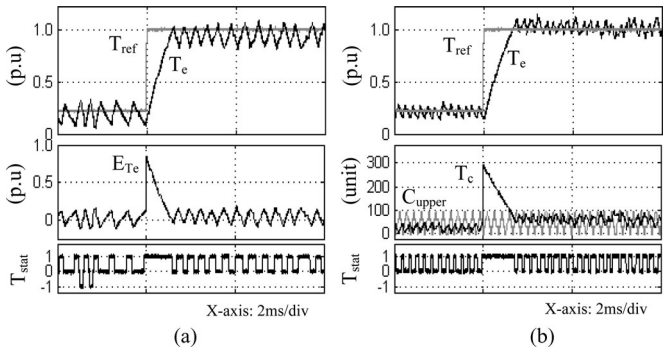

Fig. 3. Comparison by experimental of torque control operations in (a) DTC-hysteresis-based and (b) DTC-CSF-based induction motor.

simple control structure (with decoupled control structure) of hysteresis-based DTC is retained. For the sake of identification, in this paper, this scheme will be referred to as DTC-CSF. The torque error status $T_{\rm stat}$ (as shown in Fig. 2) generated from the constant frequency torque controller to compensate the torque error $E_{\rm Te}$ can be described by

$$T_{\rm stat} = \begin{cases} 1 & \text{for} \quad T_c \geq C_{\rm upper} \\ 0 & \text{for} \quad C_{\rm lower} < T_c < C_{\rm upper} \\ -1 & \text{for} \quad T_c \leq C_{\rm lower} \end{cases} \tag{1}$$

where T_c is the output of proportional-integral (PI) control and $C_{\rm upper}$ and $C_{\rm lower}$ are the upper and lower triangular carriers, respectively. In order to establish CSF and, hence, reduced torque ripple, the frequency and peak to peak of upper and lower triangular waveforms are set at fixed values. For PI torque controller, the gain values of K_p and K_i are restricted to ensure the absolute slope of the output signal, and T_c does not exceed the absolute slope of triangular carrier [36].

Fig. 3 shows the experimental results of torque control operations for a step change of torque reference from 0.22 to 1.0 p.u obtained in DTC-hysteresis-based and DTC-CSF-based induction machines. The values of machine and control system parameters are given in Table I. From Fig. 3, it can be seen that the output torque ripple in DTC-CSF is reduced and the output torque is regulated closer to the reference with a constant and higher switching frequency. In general, the output torque ripple can be decreased by increasing the frequency of the triangular carriers with proper gain setting of the PI controller. On the other hand, to increase the switching frequency and to reduce

TABLE I
INDUCTION MACHINE PARAMETERS, HYSTERESIS-BASED DTC AND CSF-BASED DTC DRIVES

1. Induction Machine			
	Stator resistance	5.5 Ω	
	Rotor resistance	4.51 Ω	
	Stator self	306.5 mH	
	Rotor self	306.5 mH	
	Mutual inductance	291.9 mH	
	Number of poles	4	
2(a). Hysteresis-based DTC		**2(b). CSF-based DTC**	
Flux hysteresis band,	0.045Wb	Flux hysteresis band,	0.045Wb
Torque hysteresis band,	0.9Nm	Flux rated	0.892Wb
Flux rated	0.892Wb	Torque rated	9Nm
Torque rated	9Nm	Constant freq. torque controller	
		Proportional gain, K_p	34
		Integral gain, K_i	11925
		Carrier frequency	3.03kH
		Peak to peak of carrier	90

the torque ripple of the DTC hysteresis-based, one can ideally reduce the hysteresis band. This may lead to the incorrect voltage vector selections (where $T_{\rm stat} = -1$) that will cause rapid decreases in output torque and hence increases the torque ripple instead of reduces it [36].

III. TORQUE CAPABILITY IN DTC

The behavior of induction machine in DTC drives can be described in terms of space vectors by the following equations written in stator flux reference frame

$$\mathbf{v}_s = r_s \mathbf{i}_s + j\omega_s \mathbf{\Psi}_s + \frac{d\mathbf{\Psi}_s}{dt} \tag{2}$$

$$0 = r_r \mathbf{i}_r + j\left(\omega_s - \omega_r\right)\mathbf{\Psi_r} + \frac{d\mathbf{\Psi_r}}{dt} \tag{3}$$

$$\mathbf{\Psi_s} = L_s \mathbf{i}_s + L_m \mathbf{i_r} \tag{4}$$

$$\mathbf{\Psi_r} = L_r \mathbf{i_r} + L_m \mathbf{i_s} \tag{5}$$

$$T_e = \frac{3}{4} p \frac{L_m}{\sigma L_s L_r} \Psi_s \Psi_r \sin\delta_{sr} \tag{6}$$

where p is the number of poles, $\delta_{\rm sr}$ is the angle between the stator flux and rotor flux vectors, ω_s is the stator flux angular frequency, ω_r is the rotor angular speed, L_s, L_r, and L_m are the motor inductances, and σ is the leakage coefficient. The leakage coefficient σ is given as

$$\sigma = 1 - \frac{L_m^2}{L_s L_r}. \tag{7}$$

In practice, a rated stator flux and inverter current limit (i.e., 150–200% of rated current machine) are used to obtain the maximum torque capability. The maximum output torque can be retained as long as the operation of rotor speed does not exceed its base speed. According to (6), the angle $\delta_{\rm sr}$ plays a vital role in controlling the output torque. Since the angle $\delta_{\rm sr}$ mainly depends on the slip angular frequency $(\omega_s - \omega_r)$, to maintain the output torque to its maximum value, the slip angular frequency $(\omega_s - \omega_r)$ must always be kept at its maximum value. This is typically established for speeds below the base speed.

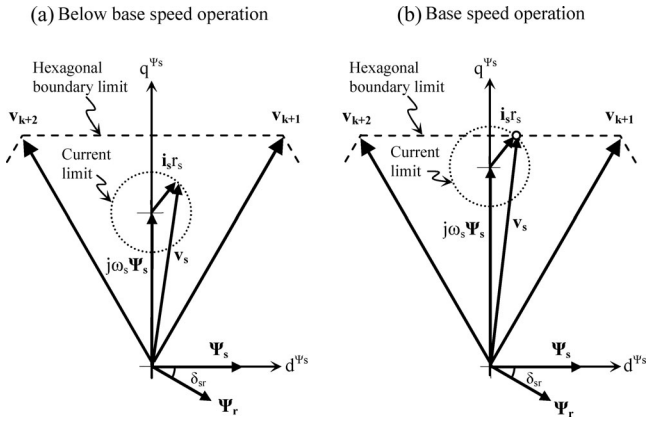

Fig. 4. Phasor diagrams at particular flux position for (a) low-speed operation and (b) high-speed operation.

Fig. 4 shows the phasor diagrams of (2) under steady-state conditions for operations below base speed [see Fig. 4(a)] and at base speed [see Fig. 4(b)]. For each case, the same magnitude of stator flux vector is used and the vectors are drawn in stator flux *d–q* reference frame. In the case of low-speed operation, the back-emf, $j\omega_s\Psi_s$ is small enough such that sufficient stator voltage can be generated to control both stator flux and torque, simultaneously. At base speed [see Fig. 4(b)], the stator voltage vector touches the hexagonal stator voltage boundary limit. Hence, there are two options to further increase the speed beyond the base and at the same time maintain the maximum torque capability.

1) Weaken the flux (in normal practice to be inversely proportional with speed), so that the magnitude of the vector $j\omega_s\Psi_s$ is retained as the frequency increases. However, the *d* component of the stator current will be reduced. Under this condition, the average stator voltage will stay on the hexagonal boundary and the stator flux is regulated using two active voltage vectors. This is what happens in the DTC hysteresis-based drive where the flux locus is circular and no overmodulation is exploited in the stator voltage.
2) Operate the inverter in overmodulation mode; thus, the average stator voltage will go beyond the hexagonal boundary limit. In normal practice, to obtain the maximum voltage vector (i.e., six-step mode), the voltage vector reference of the SVM is modified [15]. Once the six-step voltage is reached, to further increase the speed, the flux will have to be weakened. This method can be performed for the DTC based on SVM. This method cannot be applied in DTC hysteresis-based drive because no stator voltage reference is available to implement the overmodulation.

Basically both methods will ensure that $(\omega_s - \omega_r)$ is kept to the maximum value. In the first method, the zero-voltage vector is not used; hence, the angular speed of the stator flux will be

increased. As the speed is increased, a more tangential voltage vector is selected; hence, higher stator flux angular speed is achieved. In the second method, the zero-voltage vector is also not used. The angular speed of the stator flux is increased since instead of alternating between two vectors, a single voltage vector is gradually applied as the waveform gradually changes from PWM to six-step mode. The flux will only be weakened once the six-step voltage is reached. This means that in the second method, the constant torque region is extended since the voltage capability is increased.

The previous discussion indicates that the control of maximum torque for a wider speed range is very much related to the ability to extend the limit of stator flux angular frequency or the stator voltage limit. In this paper, a method that uses an overmodulation strategy is proposed. However, unlike other modulation strategies, which used SVM (the second method), the proposed method is based on the DTC hysteresis-based structure, which contains no voltage vector reference.

IV. Improved Torque Capability With the Proposed Overmodulation Strategy

This section presents the proposed overmodulation strategy to improve capability of torque over a wide speed range operation. The method is different from the SVM-based system where the reference stator voltage is available and overmodulation is achieved by modifying the reference voltage. With no reference voltage available in DTC-CSF, the overmodulation is accomplished by gradually transforming the PWM voltage waveform to six-step mode, which is achieved by transforming the shape of the stator flux locus from circular to the hexagonal shapes. Since DTC-CSF uses the same structure as the DTC hysteresis-based, the control structure is simple yet CSF and reduced torque ripple can be achieved without the need of SVM. This section will first discuss how the PWM to six-step mode operation is accomplished by shaping the stator flux locus without resolving to DTC-SVM-based drive. Next, the operation in field-weakening mode using the proposed overmodulation is described.

A. Extending the Stator Voltage Operation to Six-Step Mode

In the SVM-based system, the overmodulation starts when the reference voltage vector goes beyond the stator voltage hexagonal trajectory. The reference voltage will be modified whenever it goes outside the hexagonal limits [15]. If the modified reference voltage moves along the hexagonal trajectory, the synthesized voltage will have no zero-voltage vector. In DTC hysteresis-based drive, zero-voltage vectors will not be selected when the actual (or estimated) torque does not reach the reference torque. In order to fully utilize the dc voltage, the stator voltage magnitude has to go beyond this limit and operate in six-step mode. However, with the conventional hysteresis-based structure DTC drive, this is not possible. With regard to the stator flux locus, when the reference voltage is sinusoidal, i.e., within the hexagon, the locus of the stator flux is circular [see Fig. 5(a)]. As a matter of fact, when the stator voltage vector trajectory moves along the hexagon without any zero-voltage vector application, the stator flux locus is still circular

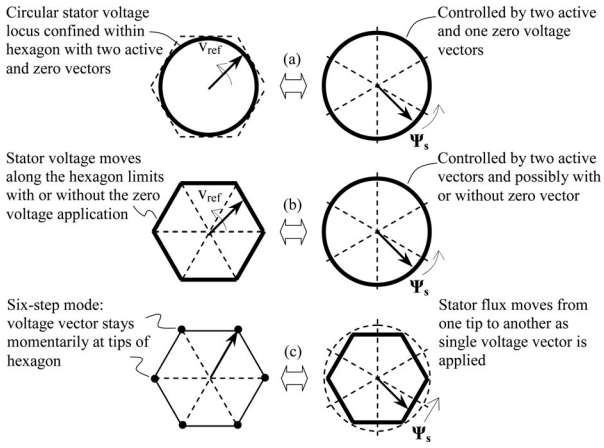

Fig. 5. Mapping of the voltage vector and the stator flux trajectories.

[see Fig. 5(b)]. This is because without the zero vectors, the stator flux is still regulated by the two active vectors and, hence, will follow the circular locus reference, with limited stator voltage and angular flux frequency. To go around this problem, what we need to do is to modify the output of the stator flux hysteresis comparator, so that the selected voltage vector will transform stator voltage to six-step waveform.

In the proposed overmodulation strategy, the stator flux locus is controlled to form the hexagonal shape during motor acceleration. By doing so, lower harmonic components in stator current due to the hexagonal flux locus and six-step operations occur but only during acceleration (or deceleration). The proposed control structure to establish the hexagonal flux locus utilizing DTC-CSF will be explained in Section V. When the motor accelerates, the back-emf increases; therefore, larger stator voltage is needed to satisfy the torque demand. The demand will be naturally fulfilled by the controller that will gradually drop the applications of zero-voltage vectors as the speed increases. As the speed is further increased and no more zero-voltage vector is available, the selection of voltage vector will naturally transform to six-step mode [see Fig. 5(c)]. In other words, by transforming the stator flux locus to the hexagonal shape, we provide the room for the stator voltage to increase beyond the hexagonal boundary and the torque demand will naturally transform the stator voltage from PWM to six-step mode.

Fig. 6 depicts the simulation results to compare the performance of stator voltage and torque capability for DTC-CSF with and without the proposed overmodulation strategy. The values of the machine and parameter systems used for both cases are given in Table I. As can be seen, a smooth transition of stator voltage from PWM to six-step mode is achieved with the proposed overmodulation strategy and hence extending the constant torque region.

B. Flux Weakening With Six-Step Mode

In the flux-weakening region, a higher capability of torque can be achieved as the proposed overmodulation strategy operates stator voltage in the six-step mode by continuously controlling the flux vector to form hexagonal locus. This paper uses a

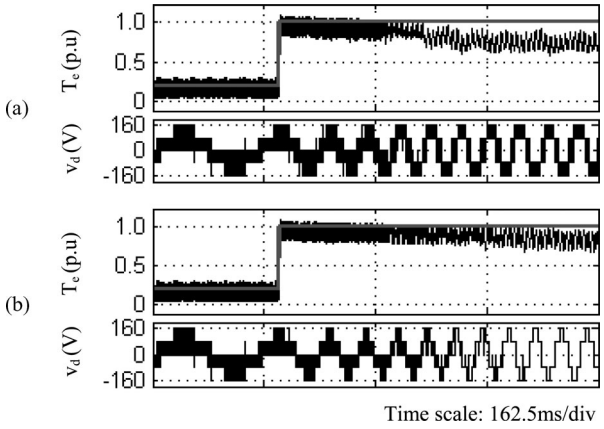

Fig. 6. Comparison of the performances of stator voltage and torque capability for (a) DTC-CSF without the proposed overmodulation and (b) DTC-CSF with the proposed overmodulation.

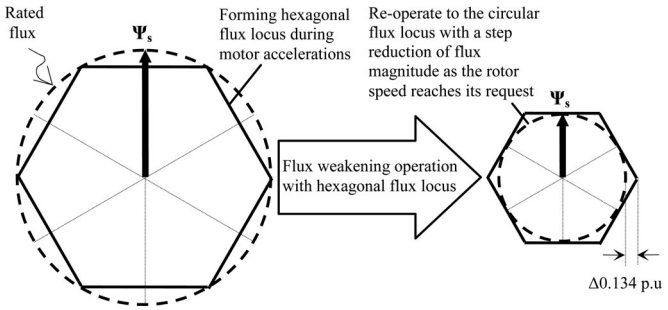

Fig. 7. Operational control of the locus and magnitude of stator flux.

conventional flux-weakening method (in order to retain the simple control structure) but with a minor modification. Using the proposed method, the magnitude of the hexagonal stator flux is inversely proportional to the rotor speed when the motor operates beyond the base speed, $\omega_{\mathrm{base,hex}}$. However, a step reduction of 13.4% in the flux magnitude is applied as the hexagonal flux locus is immediately changed back into the circular locus when the motor speed reaches its target (steady-state speed). The operational control of locus and magnitude of stator flux can be described as illustrated in Fig. 7. This reduction ensures that the output torque can be well regulated to its reference. In fact, higher level of flux reference (which for this case is without a step reduction), particularly at very high speed operations, gives insufficient stator flux angular frequency (or appropriate slip) which may degrade the output torque control, as discussed in [1]. The reference of flux is given as

$$\Psi_{s,\mathrm{ref}} = \Psi_{s,\mathrm{rated}} \frac{\omega_{\mathrm{base,hex}}}{\omega_m} \left(1 - \alpha . \cos\left(\pi/6\right)\right) \qquad (8)$$

where $\Psi_{s,\mathrm{rated}}$ is the stator flux rated and α is used to activate the step reduction when α equals 1 otherwise it is 0.

V. Proposed Control Structure

Fig. 8 shows the control structure of DTC-CSF with the proposed overmodulation strategy. Notice that all components of the DTC hysteresis-based scheme are retained, except for the inclusion of the "modification of flux error status" block which

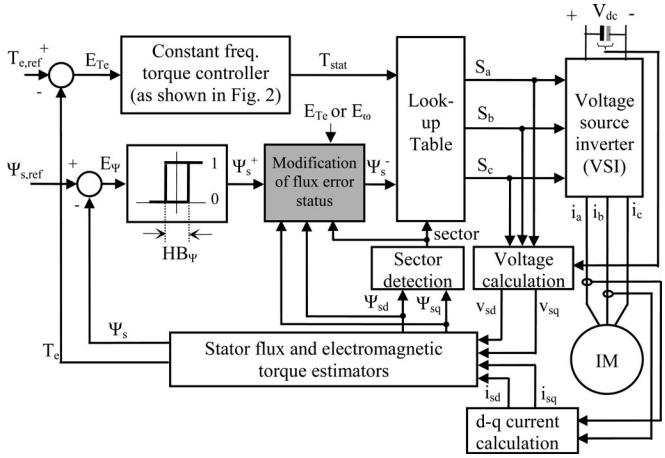

Fig. 8. Structure of DTC-CSF-based induction machine with the proposed block of modification of flux error status.

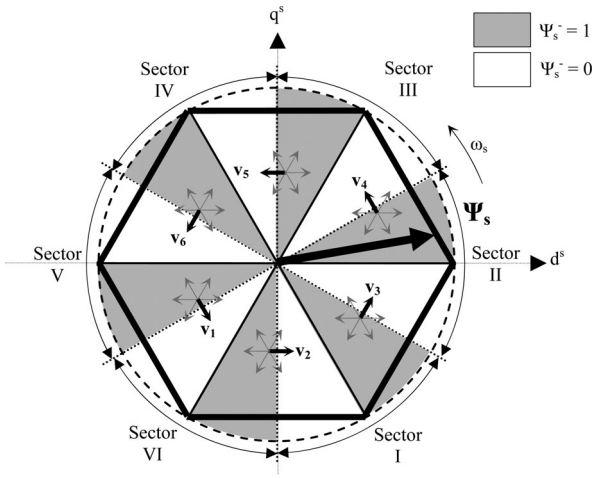

Fig. 9. Proposed digital outputs for modified flux error status corresponding to the flux positions (subsector in every sector).

is responsible for the overmodulation mode by transforming the stator flux locus from circular to hexagon. For speed control operation, the torque reference $T_{e,\mathrm{ref}}$ is generated from a PI speed controller and the reference of flux is calculated using (8) in flux weakening region or it is held at rated flux in constant torque region. The locus of stator flux is controlled to form a hexagonal shape when the motor operates under acceleration condition (i.e., by inspecting the error of rotor speed E_ω) by modifying the flux error status (Ψ_s^+) to a new flux status (Ψ_s^-) before it is being fed to the lookup table.

The proposed digital outputs of the modified flux error status Ψ_s^- (to perform hexagonal flux locus) according to flux positions are illustrated in Fig. 9. Each sector in the stator flux plane is divided into two subsectors: subsector1 (shaded area) and subsector2 (unshaded area). For example, let us consider a flux located in sector 1 and rotating in a counterclockwise direction. When the flux position is in subsector1, the "modification of flux error status" block will produce a signal that will request the flux to increase (i.e., $\mathbf{v}_2$). As the flux enters subsector 2, the block will produce a signal that will request the flux to decrease (i.e., $\mathbf{v}_3$).

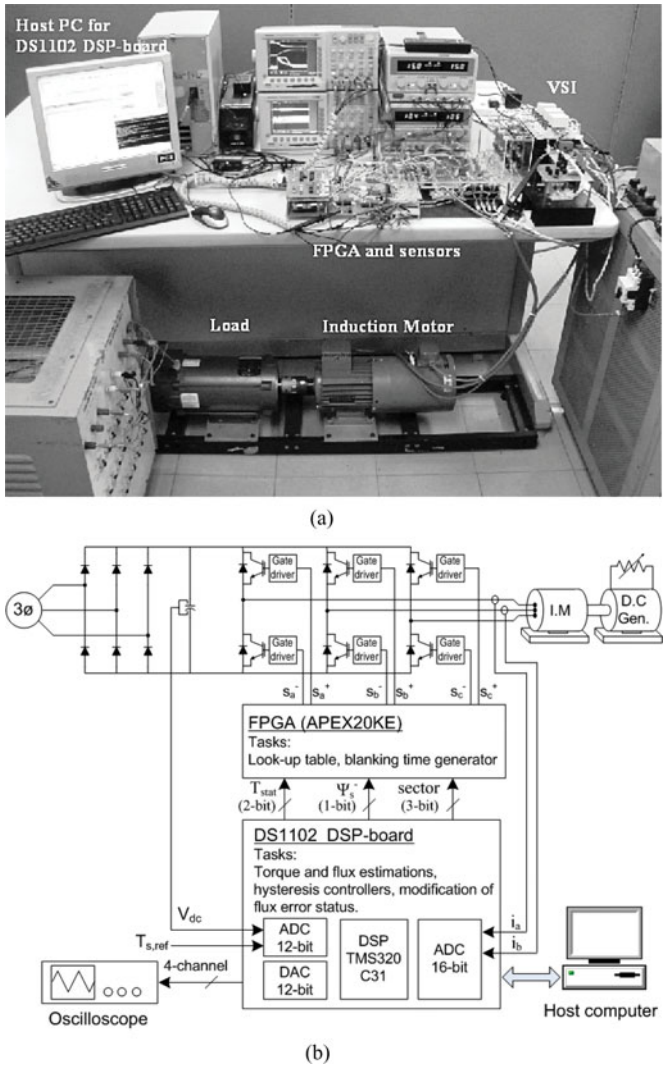

Fig. 10. Complete drive system. (a) Picture of the experiment setup. (b) Functional block diagram of the experiment setup.

This will be repeated as the flux moves to a different sector and as a result, the stator flux locus will become hexagonal. As the flux travels from one tip to another, zero vectors will be alternately selected between the active voltage vectors. However, as the rotor speed increases, less zero vector duration will be generated, and thus, this will ensure the stator flux frequency is increased to maintain the maximum torque capability.

VI. Implementation and Experimental Results

To verify the feasibility of the proposed overmodulation and flux weakening strategy, a complete drive system, as shown in Fig. 10, has been realized. The experimental setup consists of an insulated gate bipolar transistor inverter and a 1.5-kW, four-pole squirrel cage induction motor. The actual parameters of an induction motor and parameters for the hysteresis-based DTC and CSF-based DTC drives are shown in Table I. For safety reasons, the dc voltage was limited to 240 V, which means that the based speed is reduced to 570 r/min. The control algorithm is implemented on a dSPACE 1102 controller board and an Altera FPGA (APEX20KE) board. The sampling period of the DTC scheme, including the proposed overmodulation, is 55 μs.

To investigate the performance of torque capability for a wide speed range operation, a step change of speed reference from 0.5 to 2.8 p.u has been carried out for five different schemes. For convenience of identification, these schemes are referenced as follows.

1) *DTC1:* conventional hysteresis-based DTC and conventional flux-weakening method [$\alpha = 0$ in (8)].
2) *DTC2:* the hysteresis-based DTC with the proposed overmodulation strategy and conventional flux-weakening method.
3) *DTC3*: the hysteresis-based DTC with the proposed overmodulation strategy with a step reduction of flux applied when the motor speed reaches its reference in flux weakening region [$\alpha = 1$ in (8)].
4) *DSC:* the hysteresis-based direct self control (DSC) as proposed in [12] and conventional flux-weakening method.
5) *DTC-CSF2:* the CSF-based DTC with the proposed overmodulation strategy with a step reduction of flux applied when the motor speed reaches its reference in flux-weakening region [$\alpha = 1$ in (8)].

Fig. 11 shows the experimental results of motor torque, stator flux, motor speed, and stator phase voltage when the step change of reference speed is applied in DTC1, DTC2, and DTC3 (all schemes used hysteresis-based controller). From Fig. 11, it can be seen that the capability of output torque in DTC2 or DTC3 during the motor acceleration is higher than that obtained in DTC1 and hence gives faster motor acceleration. The proposed overmodulation strategy (utilized in DTC2 and DTC3), as discussed in the previous section, provides an extension of constant torque region and allows the stator voltage to operate in complete six-step mode, particularly in flux weakening region. The extension of the constant torque region in Fig. 11 can be more clearly demonstrated through torque–speed curve, as depicted in Fig. 12, which shows the plot of torque versus speed obtained from Fig. 11. The figure indicates that the constant torque region for DTC3 is increased by more than 10% when compared with DTC1. With the extension of the constant torque region, the torque capability during the field-weakening mode is also improved.

The exploitations of stator voltage in overmodulation region as well as the smooth transition from the PWM to the six-step mode in DTC2 and DTC3 are shown in Fig. 13. Fig. 13 also shows the output torque in DTC1, DTC2, and DTC3 as the motor speed approaches and reachs its target. In these cases, the data taken (i.e., in the region of "↔") are plotted using a larger scale to clearly present the effects. From this figure, it can be seen that the regulation of output torque in DTC2 is poor when the stator flux locus returns to the circular shape because of the excessive flux reference. For this reason, the step reduction of the flux amplitude as introduced in (8) is applied in DTC3 at the instant the stator flux returns to the circular locus when the reference speed is reached. By doing so, the DTC3 provides better output torque control and higher capability of torque as depicted in Fig. 13.

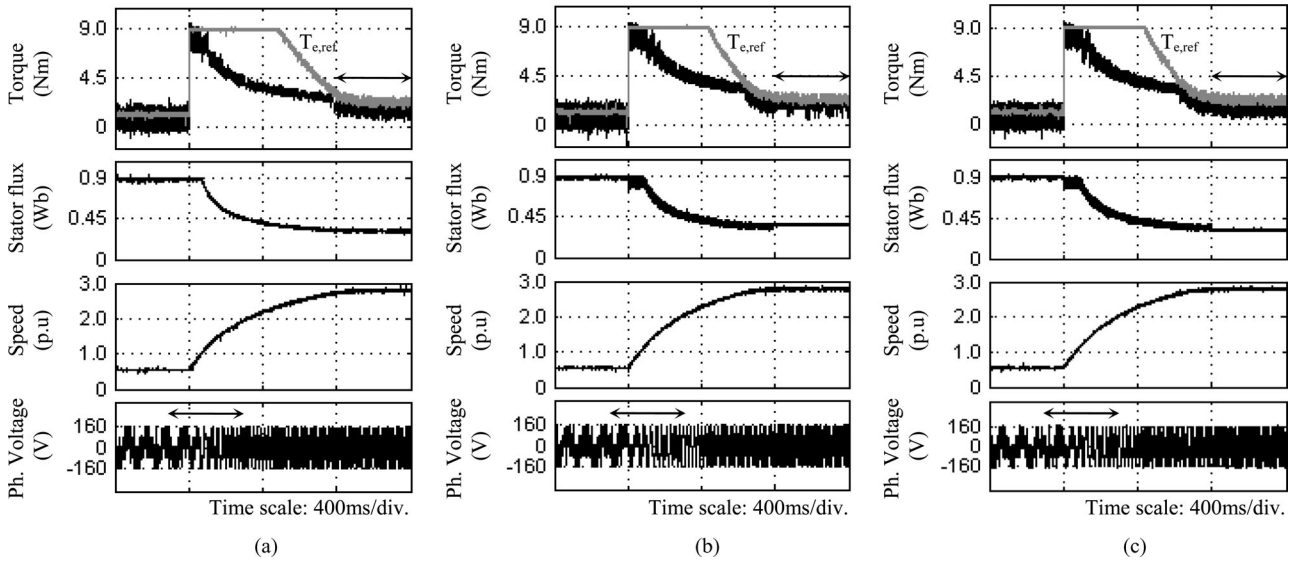

Fig. 11. Experimental results of output torque, stator flux magnitude, motor speed, and stator phase voltage when a step change of speed reference from 0.5 to 2.8 p.u is applied in (a) DTC1, (b) DTC2, and (c) DTC3.

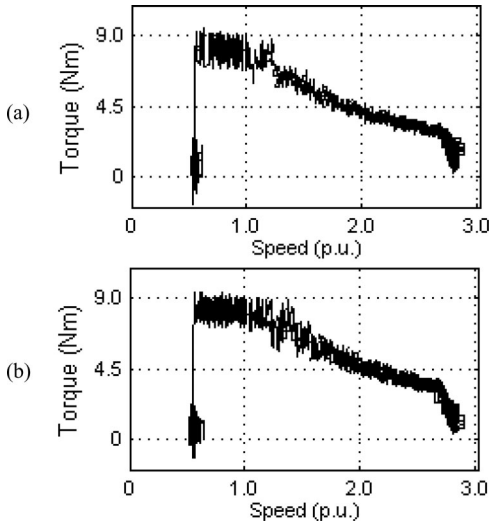

Fig. 12. Experimental graph of torque–speed for (a) DTC1 and (b) DTC3 (corresponding to the results obtained in Fig. 11).

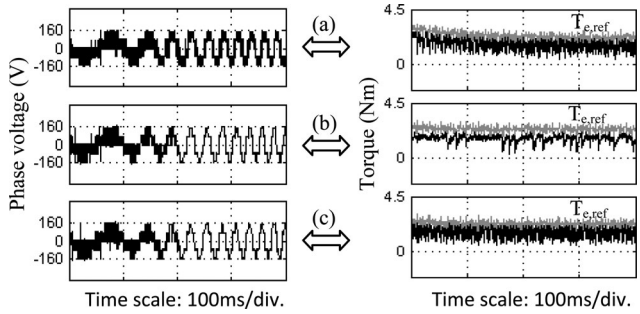

Fig. 13. Zoomed images (corresponding to the results obtained in Fig. 11) of stator phase voltage and output torque in (a) DTC1, (b) DTC2, and (c) DTC3.

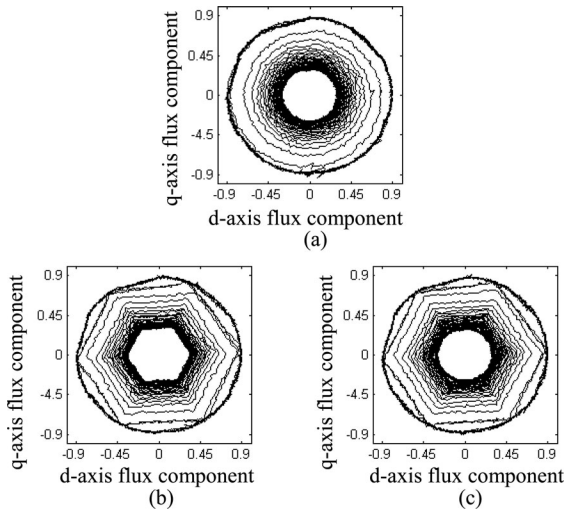

Fig. 14. Comparison of stator flux locus obtained in (a) DTC1, (b) DTC2, and (c) DTC3.

The operation of stator flux locus for DTC1, DTC2, and DTC3 corresponding to the results obtained in Fig. 11 are depicted in Fig. 14. It is apparent that the step reduction of flux magnitude proposed in DTC3 fits into the hexagonal flux locus as the motor speed reaches its reference. On the other hand, the magnitude of circular flux locus in DTC2, which is identical to the magnitude of hexagonal flux locus, gives a flux reference which is too high and hence causes poor performance of torque control at very high speed operation as shown in Figs. 11(b) and 13(b). From Fig. 14, it also can be noticed that the magnitude of the stator flux in DTC1 and DTC3 are the same as the motor speed reaches its reference.

Fig. 15 depicts the experimental results of motor torque, stator flux, motor speed, and stator current when the step change of reference speed is applied in DTC3, DSC, and DTC-CSF2. From Fig. 15, it can be observed that the capabilities of torque obtained in these schemes, during motor accelerations, are comparable to the flux locus that forms into the hexagonal shape. Although the DSC is known to offer superior dynamic performance, this scheme produces high currents total harmonic distortions (THD)

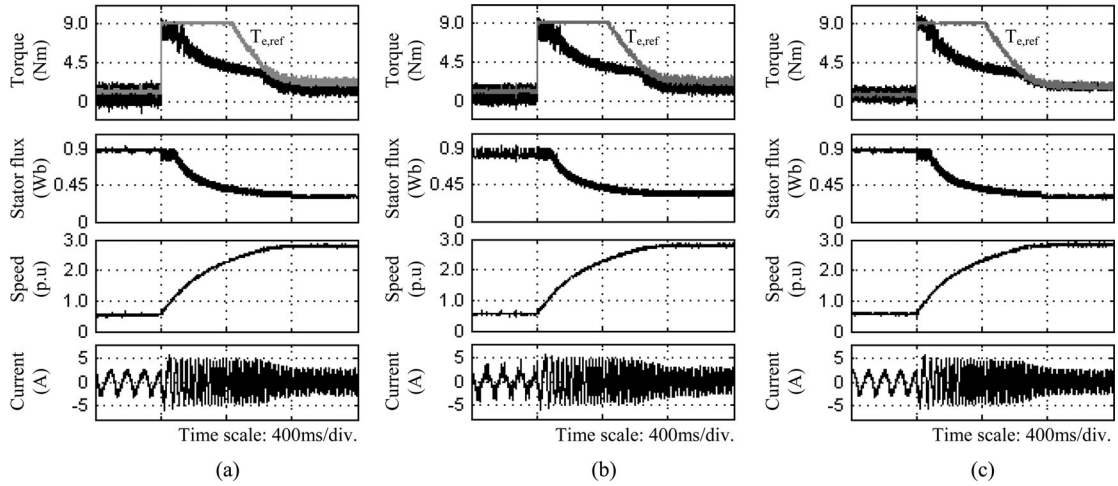

Fig. 15. Experimental results of output torque, stator flux magnitude, motor speed, and stator current when a step change of speed reference from 0.5 to 2.8 p.u is applied in (a) DTC3, (b) DSC, and (c) DTC-CSF2.

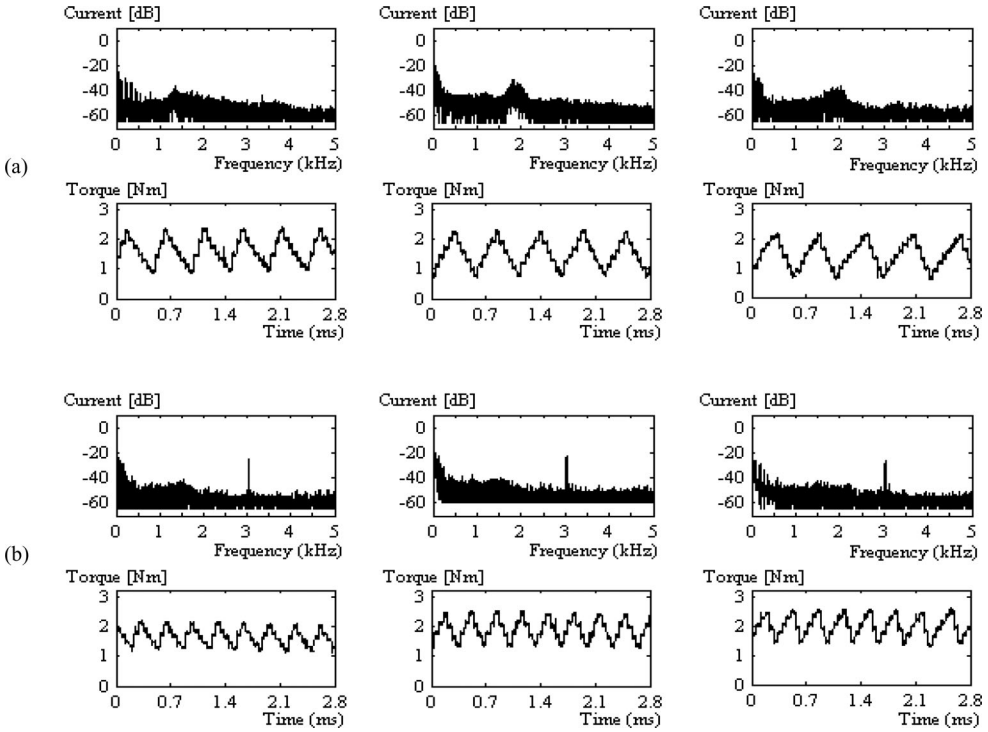

Fig. 16. Experimental results of phase current frequency spectrum and output torque for (a) basic DTC and (b) DTC-CSF at the speed of approximately 20, 30, and 55 rad/s.

even operating in steady-state conditions. As can be seen from Fig. 15(b), the stator current in DSC seems to have high THD (obviously as the motor speed runs at 0.5 p.u) since the flux locus is always hexagonal. In Fig. 15, it also can be noted that the DTC-CSF2 offers lower output torque ripple when the output torque is controlled at its reference.

Fig. 16 shows the frequency spectrum of the phase current obtained from the experimental results for the basic DTC and DTC-CSF at the speed of 20, 30, and 55 rad/s, while the output torque is controlled at 2 Nm. It can be seen that the phase current in DTC-CSF contains dominant harmonic at triangular frequency (i.e., at 3.03 kHz) regardless of the speed, as opposed to the DTC hysteresis-based which has a frequency spectrum which is spread out and depends on the operating speed.

VII. Conclusion

An overmodulation strategy for DTC-CSF-based induction machine drives is proposed to achieve higher capability of torque for a wider speed range operation. In this way, the hexagonal flux locus is operated to allow the stator voltage increases up to six-step mode as the rotor speed increases, in constant torque region. In addition, the proposed overmodulation employed in DTC-CSF offers improved performance of torque control and

reduced torque ripple. The main benefit of the proposed strategy is its simplicity since the proposed control structure does not require a SVM modulator normally employed for overmodulation operation.

ACKNOWLEDGMENT

The authors would like to thank the Ministry of Science, Technology and Innovation, Universiti Teknikal Malaysia Melaka and Universiti Teknologi Malaysia for providing the funding, sponsorship and laboratory facilities for this research.

REFERENCES

[1] X. Xu and D. W. Novotny, "Selection of the flux reference for induction machine drives in the field weakening region," *IEEE Trans. Ind. Appl.*, vol. 28, no. 6, pp. 1353–1358, Nov./Dec. 1992.

[2] O. Wasynczuk, S. D. Sudhoff, K. A. Corzine, J. L. Tichenor, P. C. Krause, I. G. Hansen, and L. M. Taylor, "A maximum torque per ampere control strategy for induction motor drives," *IEEE Trans. Energy Convers.*, vol. 13, no. 23, pp. 163–169, Jun. 1998.

[3] K. Sang-Hoon and S. Seung-Ki, "Maximum torque control of an induction machine in the field weakening region," *IEEE Trans. Ind. Appl.*, vol. 31, no. 4, pp. 787–794, Jul./Aug. 1995.

[4] S. Myoung-Ho, H. Dong-Seok, and C. Soon-Bong, "Maximum torque control of stator-flux-oriented induction machine drive in the field-weakening region," *IEEE Trans. Ind. Appl.*, vol. 38, no. 1, pp. 117–122, Jan./Feb. 2002.

[5] M. Mengoni, L. Zarri, A. Tani, G. Serra, and D. Casadei, "Stator flux vector control of induction motor drive in the field weakening region," *IEEE Trans. Power Electron.*, vol. 23, no. 2, pp. 941–949, Mar. 2008.

[6] S. Jul-Ki and S. Seung-Ki, "Optimal flux selection of an induction machine for maximum torque operation in flux-weakening region," *IEEE Trans. Power Electron.*, vol. 14, no. 4, pp. 700–708, Jul. 1999.

[7] H. Grotstollen and J. Wiesing, "Torque capability and control of a saturated induction motor over a wide range of flux weakening," *IEEE Trans. Ind. Electron.*, vol. 42, no. 4, pp. 374–381, Aug. 1995.

[8] D. Casadei, G. Serra, and A. Tani, "Direct flux and torque control of induction machine for electric vehicle applications," in *Proc. 7th Int. Conf. Electr. Mach. Drives*, Sep. 1995, pp. 349–353.

[9] D. Casadei, G. Serra, A. Stefani, A. Tani, and L. Zarri, "DTC drives for wide speed range applications using a robust flux-weakening algorithm," *IEEE Trans. Ind. Electron.*, vol. 54, no. 5, pp. 2451–2461, Oct. 2007.

[10] H. Abu-Rub, H. Schmirgel, and J. Holtz, "Maximum torque production in rotor field oriented control of an induction motor at field weakening," in *Proc. IEEE Int. Symp Ind. Electron.*, Jun. 2007, pp. 1159–1164.

[11] H. Abu-Rub, H. Schmirgel, and J. Holtz, "Sensorless control of induction motors for maximum steady-state torque and fast dynamics at field weakening," in *Proc. 41st IAS Annu. Meet. Conf. Record Ind. Appl. Conf.*, Oct. 2006, pp. 96–103.

[12] M. Depenbrock, "Direct self-control (DSC) of inverter-fed induction machine," *IEEE Trans. Power Electron.*, vol. 3, no. 4, pp. 420–429, Oct. 1988.

[13] A. Tripathi, A. M. Khambadkone, and S. K. Panda, "Dynamic control of torque in overmodulation and in the field weakening region," *IEEE Trans. Power Electron.*, vol. 21, no. 4, pp. 1091–1098, Jul. 2006.

[14] G. Gallegos-Lopez, F. S. Gunawan, and J. E. Walters, "Current control of induction machines in the field-weakened region," *IEEE Trans. Ind. Appl.*, vol. 43, no. 4, pp. 981–989, Jul./Aug. 2007.

[15] J. Holtz, W. Lotzkat, and A. M. Khambadkone, "On continuous control of PWM inverters in the overmodulation range including the six-step mode," *IEEE Trans. Power Electron.*, vol. 8, no. 4, pp. 546–553, Oct. 1993.

[16] T. G. Habetler, F. Profumo, M. Pastorelli, and L. M. Tolbert, "Direct torque control of induction machines using space vector modulation," *IEEE Trans. Ind. Appl.*, vol. 28, no. 5, pp. 1045–1053, Sep./Oct. 1992.

[17] A. Tripathi, A. M. Khambadkone, and S. K. Panda, "Stator flux based space-vector modulation and closed loop control of the stator flux vector in overmodulation into six-step mode," *IEEE Trans. Power Electron.*, vol. 19, no. 3, pp. 775–782, May 2004.

[18] G. Griva, T. G. Habetler, F. Profumo, and M. Pastorelli, "Performance evaluation of a direct torque controlled drive in the continuous PWM-square wave transition region," *IEEE Trans. Power Electron.*, vol. 10, no. 4, pp. 464–471, Jul. 1995.

[19] A. M. Khambadkone and J. Holtz, "Compensated synchronous PI current controller in overmodulation range and six-step operation of space-vector-modulation-based vector-controlled drives," *IEEE Trans. Ind. Electron.*, vol. 49, no. 3, pp. 574–580, Jun. 2002.

[20] J. O. P. Pinto, B. K. Bose, L. E. B. Da Silva, and M. P. Kazmierkowski, "A neural-network-based space-vector PWM controller for voltage-fed inverter induction motor drive," *IEEE Trans. Ind. Appl.*, vol. 36, no. 6, pp. 1628–1636, Nov./Dec. 2000.

[21] C. Lascu, I. Boldea, and F. Blaabjerg, "A modified direct torque control for induction motor sensorless drive," *IEEE Trans. Ind. Appl.*, vol. 36, no. 1, pp. 122–130, Jan./Feb. 2000.

[22] D. Casadei, G. Serra, and K. Tani, "Implementation of a direct control algorithm for induction motors based on discrete space vector modulation," *IEEE Trans. Power Electron.*, vol. 15, no. 4, pp. 769–777, Jul. 2000.

[23] I. Takahashi and T. Noguchi, "A new quick-response and high-efficiency control strategy of an induction motor," *IEEE Trans. Ind. Appl.*, vol. IA-22, no. 5, pp. 820–827, Sep. 1986.

[24] K. Jun-Koo, C. Dae-Woong, and S. Seung-Ki, "Direct torque control of induction machine with variable amplitude control of flux and torque hysteresis bands," in *Proc. Int. Conf. Electr. Mach. Drives*, May 1999, pp. 640–642.

[25] V. Ambrozic, G. S. Buja, and R. Menis, "Band-constrained technique for direct torque control of induction motor," *IEEE Trans. Ind. Electron.*, vol. 51, no. 4, pp. 776–784, Aug. 2004.

[26] T. Noguchi, M. Yamamoto, S. Kondo, and I. Takahashi, "Enlarging switching frequency in direct torque-controlled inverter by means of dithering," *IEEE Trans. Ind. Appl.*, vol. 35, no. 6, pp. 1358–1366, Nov./Dec. 1999.

[27] S. Mir and M. E. Elbuluk, "Precision torque control in inverter-fed induction machines using fuzzy logic," in *Proc. 26th Annu. IEEE Power Electron. Spec. Conf.*, Jun. 1995, vol. 1, pp. 396–401.

[28] K. Jun-Koo and S. Seung-Ki, "New direct torque control of induction motor for minimum torque ripple and constant switching frequency," *IEEE Trans. Ind. Appl.*, vol. 35, no. 5, pp. 1076–1082, Sep./Oct. 1999.

[29] A. Tripathi, A. M. Khambadkone, and S. K. Panda, "Torque ripple analysis and dynamic performance of a space vector modulation based control method for AC-drives," *IEEE Trans. Power Electron.*, vol. 20, no. 2, pp. 485–492, Mar. 2005.

[30] J. Rodriguez, J. Pontt, C. Silva, R. Huerta, and H. Miranda, "Simple direct torque control of induction machine using space vector modulation," *Electron. Lett.*, vol. 40, pp. 412–413, 2004.

[31] D. Casadei, G. Serra, A. Tani, L. Zarri, and F. Profumo, "Performance analysis of a speed-sensorless induction motor drive based on a constant-switching-frequency DTC scheme," *IEEE Trans. Ind. Appl.*, vol. 39, no. 2, pp. 476–484, Mar./Apr. 2003.

[32] J. Beerten, J. Verveckken, and J. Driesen, "Predictive direct torque control for flux and torque ripple reduction," *IEEE Trans. Ind. Electron.*, vol. 57, no. 1, pp. 404–412, Jan. 2010.

[33] T. Geyer, G. Papafotiou, and M. Morari, "Model predictive direct torque control—Part I: Concept, algorithm, and analysis," *IEEE Trans. Ind. Electron.*, vol. 56, no. 6, pp. 1894–1905, Jun. 2009.

[34] G. Papafotiou, J. Kley, K. G. Papadopoulos, P. Bohren, and M. Morari, "Model predictive direct torque control—Part II: Implementation and experimental evaluation," *IEEE Trans. Ind. Electron.*, vol. 56, no. 6, pp. 1906–1915, Jun. 2009.

[35] G. Abad, M. A. Rodriguez, and J. Poza, "Two-level VSC based predictive direct torque control of the doubly fed induction machine with reduced torque and flux ripples at low constant switching frequency," *IEEE Trans. Power Electron.*, vol. 23, no. 3, pp. 1050–1061, May 2008.

[36] N. R. N. Idris and A. H. M. Yatim, "Direct torque control of induction machines with constant switching frequency and reduced torque ripple," *IEEE Trans. Ind. Electron.*, vol. 51, no. 4, pp. 758–767, Aug. 2004.

Auzani Bin Jidin (M'07) received the B.Eng. and M.Eng. degrees in electrical engineering from Universiti Teknologi Malaysia, Skudai, Malaysia, in 2002 and 2004, respectively, and where he is currently working on the Ph.D. degree.

He is a Lecturer at Universiti Teknikal Malaysia Melaka (UTeM), Melaka, Malaysia. He is with the Department of Power Electronics and Drives, Faculty of Electrical Engineering, UTeM. His research interests include the field of power electronics, motor drive systems, field programmable gate array, and digital signal processing applications.

Nik Rumzi Bin Nik Idris (M'97–SM'03) received the B.Eng. degree in electrical engineering from the University of Wollongong, Wollongong, Australia, the M.Sc. degree in power electronics from Bradford University, Bradford, West Yorkshire, U.K., and the Ph.D. degree from Universiti Teknologi Malaysia, Skudai, Malaysia, in 1989, 1993, and 2000, respectively.

He was a Visiting Research Associate at the University of Akron, Akron, OH, in 2002. Currently, he is an Associate Professor at the Universiti Teknologi Malaysia. His research interests include ac drive systems and digital signal processing applications in power electronic systems.

Dr. Idris is an Administrative Committee Member of the Industry Applications Society, Power Electronics Society, and Industrial Electronics Society Joint Chapter of IEEE Malaysia Section.

Abdul Halim Bin Mohamed Yatim (M'89–SM'01) received the B.Sc. degree in electrical and electronic engineering from Portsmouth Polytechnic, Portsmouth, U.K., in 1981, and the M.Sc. and Ph.D. degrees in power electronics from Bradford University, Bradford, U.K., in 1984 and 1990, respectively.

Since 1982, he has been a member of the Faculty at the Universiti Teknologi Malaysia, Skudai, Malaysia, where he is currently a Professor and Deputy Dean of the Faculty. He has been involved in several research projects in the areas of power electronic applications and drives. He was a Commonwealth Fellow during 1994–1995 at Heriot-Watt University, Edinburgh, U.K., and a Visiting Scholar at the Virginia Power Electronics Center, Virginia Polytechnic Institute and State University, Blacksburg, in 1993.

Dr. Yatim is a Corporate Member of the Institution of Engineers Malaysia. He is a Registered Professional Engineer with the Malaysian Board of Engineers. He currently holds the Interim Chapter Chair of the Malaysian Section of the IEEE Industrial Electronics/Industry Applications/Power Electronics Joint Societies.

Malik E. Elbuluk (S'79–M'79–SM'97) received the B.Sc. (Hons.) degree from the University of Khartoum, Khartoum, Sudan, and the M.S., E.E., and D.Sc. degrees from the Massachusetts Institute of Technology, Cambridge, in 1976, 1980, 1981, and 1986, respectively, all in electrical engineering.

He is currently a Professor at the University of Akron, Akron, OH, where he has been since 1989. He was with the Faculty of the Department of Electrical and Computer Engineering and the Electric Power Research Center, North Carolina State University, from 1986 to 1989. He was a Summer Research Fellow at NASA Lewis Research Center, Cleveland, OH, from 1991 to 2000. His work at NASA included low-temperature electronics for space missions, modeling and simulation of the Space Station Freedom, the power by wire, the power electronic building blocks, and the starter/generator for aircraft engines and sensorless control of electromechanical actuators for the more electric aircraft. His teaching and research interests include the areas of power electronics, electric machines, control systems, fuzzy logic, and neural networks.

Prof. Elbuluk actively publishes and reviews papers for IEEE Conferences and Transactions, and has organized and chaired a number of sessions for the Power Electronics, the Industry Application, and the Industrial Electronics Societies. He was an Associate Editor for the IEEE TRANSACTIONS IN POWER ELECTRONICS and is currently the Manufacturing Systems Development and Applications Department Vice President for the IEEE TRANSACTIONS ON INDUSTRY APPLICATIONS and also the Vice President and Technical Program Chair for the Industry Automation and Control Committee. He is a Registered Professional Engineer in the Ohio.

Tole Sutikno (M'07) received the B.Eng. degree in electrical engineering from Diponegoro University, Semarang, Indonesia, the M.Eng. degree in power electronics from Gadjah Mada University, Yogyakarta, Indonesia, in 1999 and 2004, respectively. He is currently working toward the Ph.D. degree in the Department of Energy Conversion, Universiti Teknologi Malaysia, Skudai, Malaysia.

Since 2001, he has been a Lecturer in the Department of Electrical Engineering, Universitas Ahmad Dahlan, Yogyakarta, Indonesia. His research interests include the field of power electronics, motor drive systems and field programmable gate array applications.